Chapter 3

3. Research Methodology and Numerical Model Formulation

3.1 General

The research methodology used in this study broadly consisted of three components: (i) Simulation of the chain pillar loading, (ii) estimation of the strength of the pillar, and (iii) determination of factor of safety for optimum design of chain pillars.

After the extraction of the coal seam, the strata above the excavated panel get de-stressed, and the redistributed overburden load is transferred to the side and front abutments. The height of the de-stressed zone (HDZ) is generally equivalent to the combined thickness of the caved and Fractured zones above the excavated panel roof (Rezaei et al., 2015a). Accurate estimation of the thickness of these zones is essential for estimating the redistributed load on the chain pillars. The selection of suitable constitutive models and the estimation of governing properties are equally important. Load on the pillar is also influenced by the abutment angle, which requires the consideration of geo-mechanical and geo-mining parameters. Reflection of the influence of the contact surfaces at the pillars and their post-failure behaviour in different material models are crucial for accurately estimating the pillar strength.

The design criterion in this study considers that the functional objective of the chain pillar is to provide isolation between longwall panels and can be allowed to have its gradual failure after extraction of both the adjoining panels. The approach of the chain pillar design covers the following:

- Field representative behaviour of the Caved zone, Fractured zone and Continuous Deformation zone
- A standard method for estimation of model parameters

- Estimation of the abutment angle for various geo-mining conditions
- Analysis of peak and post-peak strengths of the pillar with different w/h ratios.
- A criterion for the optimum design of the chain pillar
- Validation of findings

A series of numerical modelling studies have been carried out to investigate these aspects of the chain pillar design. The final model is developed considering the outcomes of all these studies to estimate the safety factor of a chain pillar under different geo-mining conditions. A parametric study has been undertaken, considering the prevailing geo-mining conditions and future longwall workings in different coalfields. The results of the study were used to develop governing equations and compare the outcome with prevalent practices in the field. The overall results have also been verified by site-specific studies of the stress transfer, pillar failure mechanism and surface subsidence profile.

3.2 Formulation of Numerical Models

Figure 3.1 shows the various numerical models and their mutual linkage as worked out in this study. Model I considered the two-dimensional plane strain condition of the vertical section of a longwall working along the face length beyond the zone of the rear abutment in the goaf to evaluate the chain pillar stability (Figure 3.2). The zone of interest in the model is comprised of the two adjacent longwall workings and the intervening chain pillars. Single and double rows of rectangular chain pillars have been considered in this study. Model II considered the the numerical simulation of the scaled down goaf material while model III was used to workout strata softening parameters of coal for different w/h ratio of the pillars.

Model IV considered three-dimensional modelling of longwall workings to replicate the progressive caving and develop a method for assessing the abutment angle in varying geo-mining conditions. Model V considered the failed and stable pillars in Indian geo-mining conditions to establish a criterion to design optimum size chain pillars. Model VI considered plane-strain modelling of a single longwall panel to simulate the fractured and Continuous Deformation zones over the caved goaf due to longwall extraction and obtaining the field representative estimates of their strength and deformation properties.

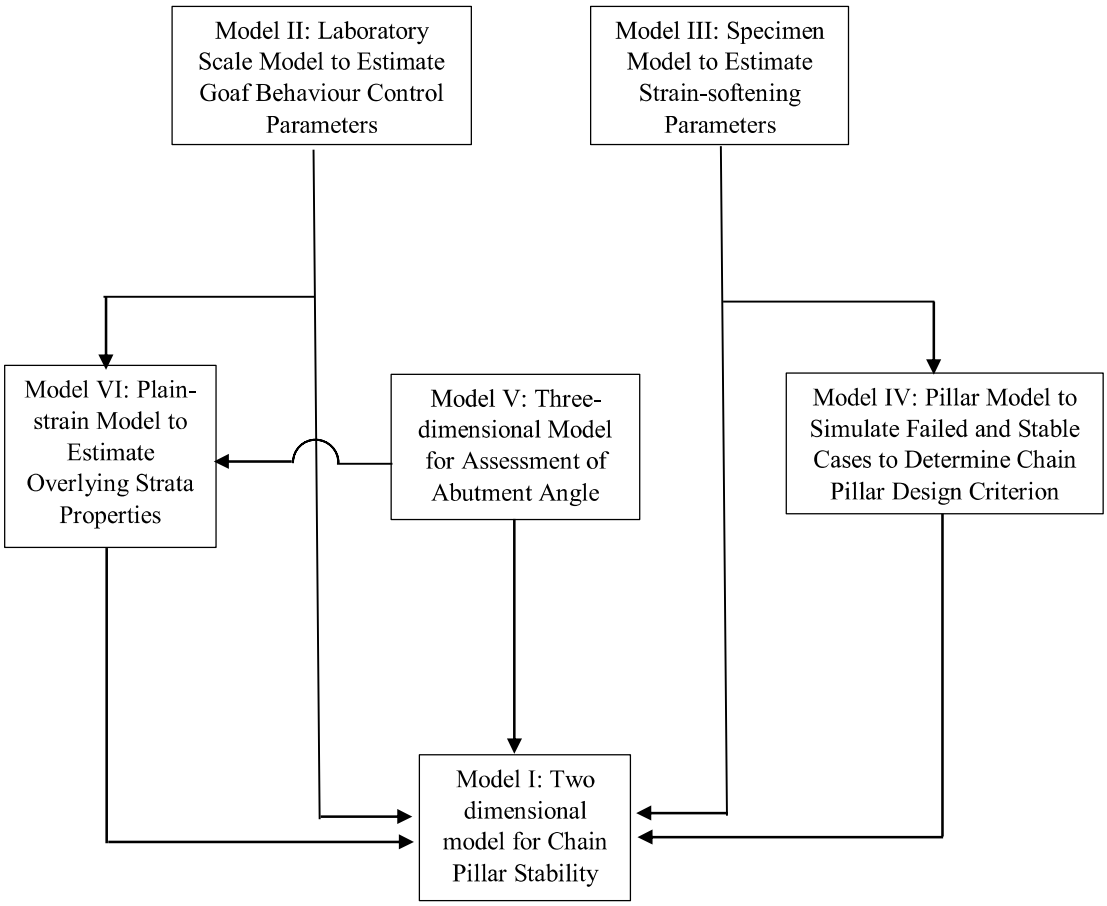

Figure 3.1 Flow chart showing the linkage between various numerical models, the outcomes of the model at the tail of the arrow line were utilised as the input for the model at the head.

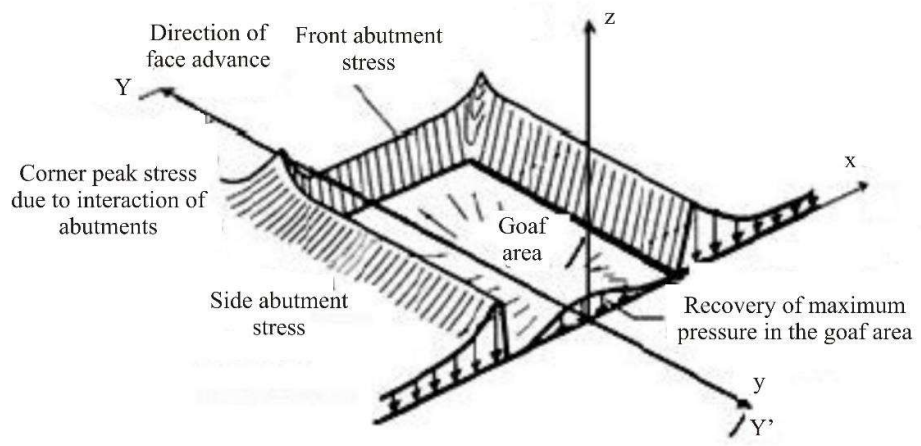

Figure 3.2 Generic layout of a longwall working showing the plane of consideration XZ in Model I

The findings and understanding developed from models II-VI were utilised for evaluating the chain pillar stability in model I. The Finite-Difference software FLAC^{3D} version 5.01 (Itasca, 2015) was employed in this study.

3.3 Assessment of Roof Layers and their Mechanical Properties

The caving of the sedimentary rock formation mainly involves the parting plane controlled caving mechanism. These parting planes or prominent layers of the separation were identified using the Roof Separation Index (RSI) (Singh and Singh, 2004). The roof strata up to 15 times the extraction height were identified for this purpose, considering the worst possible extent of the active caving zone in the Indian geo-mining conditions. The RSI includes six parameters: Uniaxial compressive strength (UCS), Rock Quality Designation (RQD), Average core length, Groundwater condition, Bed thickness, and the types of rock formation of the bed (Table AI.1).

The RSI of a bed is calculated as the algebraic summation of the ratings of these parameters. As per the standard criteria, the rock beds with RSI≤14 acted as the separation layer in the sequence of the rock beds.

The rock beds between the separation layers are combined to form roof layers. The beds beyond the active caving zone formed the overburden. The strength properties and RQD of these layers were estimated as their thickness weighted values. The elastic modulus of a layer was calculated using Equation 3.1.

$$E = \frac{\sum_{i=1}^{n} t_i}{\sum_{i=1}^{n} \frac{t_i}{E_i}} \tag{3.1}$$

where E is the elastic modulus of the layer, t_i and E_i represent the thickness and the elastic modulus of the ith rock bed.

3.4 Simulation of Parting Planes

The parting planes are simulated using built-in interface elements, representing the planes along which sliding and separation can occur during the bending of the layers. The interfaces in FLAC^{3D} are one-sided and represented as collections of triangular elements attached to a target face of the zone surface, where two triangular interface elements are defined for each quadrilateral zone face. The contact of another zone face is detected at the interface node as defined by the elastic stiffness and sliding properties characterised by Coulomb sliding and tensile bonding. The material properties of the interfaces include normal and shear stiffness, shear bonding controlled by friction, cohesion and dilation, and tensile bond strength. The absolute normal displacement and relative shear velocity are calculated at every interface node and its target face during each time step. The normal and shear force vectors are then calculated by substituting these values in the interface constitutive model. The Coulomb shear-strength

criterion limits the shear force acting at an interface node. In contrast, the dilation angle increases the effective normal stress at the target face after attaining the shear-strength limit. Figure 3.2 shows the components of the constitutive model at the interface nodes.

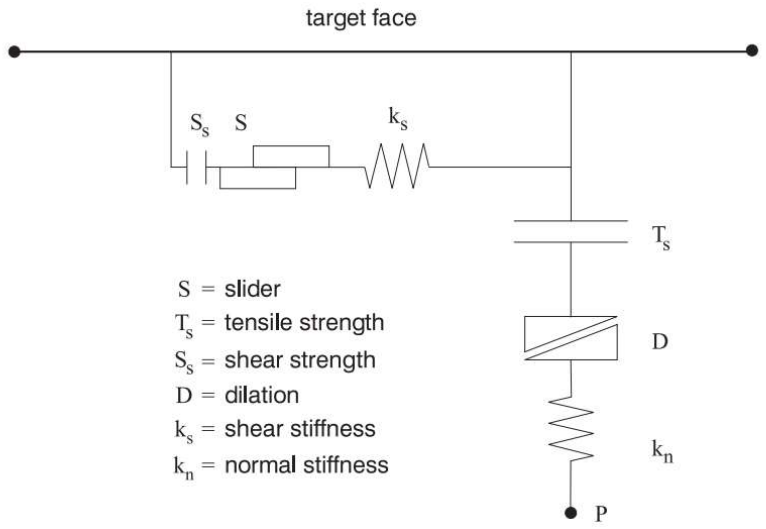

Figure 3.3 Schematic diagram depicting the component of the constitutive model of an interface node (Itasca, 2015)

The selection of material properties of the interface depends on its purpose of use. It may be used to represent an actual interface which can slip or open up due to the expected loading, but the normal displacement (interpenetration) is not important. For example, the interfaces used to represent the contact surface between platens and the samples in the compression test set-up. In such cases, the elastic stiffness properties are not that important; rather, the strength properties of the interface govern the behaviour of the system (Interface type - I). Nevertheless, the stiffness of the interface cannot be set at a very high value, which leads to a prolonged model response and delayed convergence of solution due to the stiffness-based mass scaling (Itasca, 2015). The software manual suggests a rule of thumb that the interface stiffness should

be set to 10 times the equivalent stiffness of the neighbouring stiffest zone (Equation 3.2). If the material on one side of the interface is much softer than that on the other side, the deformation of the entire system is dominated by the softer side. Therefore, reckoning the interface stiffness as ten times the stiffness of the softer side ensures minimal influence on the system compliance. The other material properties such as friction, cohesion, dilation and tensile strength are determined from direct shear tests.

$$max\left[\frac{\left(K+\frac{4}{3}G\right)}{\Delta z_{min}}\right] \tag{3.2}$$

where K and G are bulk and shear moduli, respectively, and Δz_{min} is the smallest width of the neighbouring zone in the normal direction (Fig. 3.3).

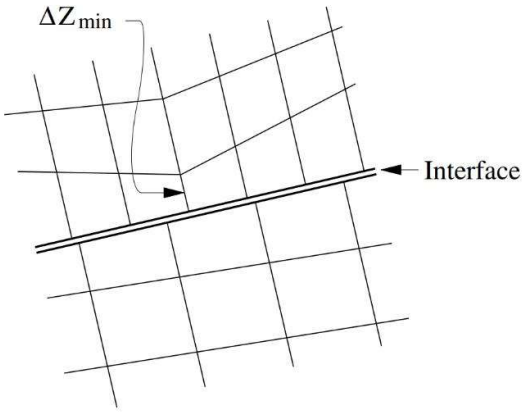

Figure 3.4 Consideration of zone dimension for interface stiffness (Itasca, 2015)

For the interface representing the soft parting plane (Interface type - II), which can influence the behaviour of the whole system, all material properties, including its elastic stiffness properties, have a physical significance. In this case, low stiffness results in the interpenetration of the nodes, giving erroneous results. The manual suggests that such interpenetration should not exceed 10% of the minimum size of the neighbouring zone. A rough estimate of the

anticipated maximum normal displacement can be made by considering the maximum induced stress and the normal stiffness, thus optimising the stiffness values to contain the maximum possible displacement within the prescribed limit (Singh, 2007).

3.5 Constitutive Model

The constitutive behaviour of the rocks depends upon their formation, state of stress relative to their strength, and the presence of fractures and joints. Additionally, the rocks are subjected to different degrees of damage depending on their position with respect to the excavation. Consequently, the constitutive behaviour of the rocks also varies. Table 3.1 summarises the constitutive models to simulate different behavioural aspects of the rocks in the numerical models.

Table 3.1 Constitutive models for different rock behaviour

Model	Rock material	Application
Null	void	excavations such as gate roads and goaf area
Isotropic elastic	homogeneous, isotropic continuum; linear stress-strain behaviour	Undamaged rocks before mining and rocks subjected to loads below their strength limit
Transversely isotropic elastic	stratified rock layers exhibiting elastic anisotropy	Stratified rocks loaded below their strength limit, especially Continuous Deformation zone rocks
Mohr-Coulomb (MC)	loose and cemented granular materials	Rocks subjected to load beyond their strength limit
MC Strain-softening	granular materials that exhibit non-linear softening	Coal and rock in their post-failure stage such as coal pillars
Ubiquitous joint	Stratified material exhibiting strength anisotropy	Rocks in the Fractured zone
Double-yield	Lightly cemented granular material in which pressure causes permanent volume decrease	Caved rocks in the goaf area

The ‘null’ model represents the material which is removed or excavated in the model. The stresses are automatically set to zero in this model. In this study, this model was assigned to the developed gate roads and the excavated panels.

The stress and strain in the ‘Elastic’ model are related according to Hooke’s law (Equation 3.3). The stress-strain rules used in this model are path-independent and linear.

$$\Delta\sigma_1 = 2G\Delta\epsilon_{ij} + \alpha_2\Delta\epsilon_{kk}\delta_{ij} \tag{3.3}$$

where δ_{ij} is the Kronecker delta symbol, $\alpha_2 = K - \frac{2}{3}G$, and K and G are bulk and shear moduli.

In the transversely isotropic model, the elastic properties in the plane of isotropy (say the local axes ‘1’ and ‘2’ lying in the same plane) are independent of that in the normal to the plane (say local axis ‘3’). The plane of isotropy is defined by the dip direction (dd) and dip angle (dip) of the plane. Young’s modulus (e1) and Poisson’s ratio (nu12) are required as input parameters to define the elastic properties in the plane, whereas shear modulus (g13) along with Young’s modulus (e3) and Poisson’s ratio (nu13) are required to characterise the elastic behaviour in any plane normal to the isotropy plane.

The plasticity models potentially encompass some degree of path-dependent permanent deformation due to the non-linear nature of the stress-strain relation. The characterisation of the different models includes yield function, flow rule and softening functions. The yield function of a model defines the stress combinations for which plastic flow would occur. The total strain increments are composed of elastic and plastic strain increments based on the assumptions of the plasticity theory. The direction of the plastic strain increments is normal to the potential plastic surface as defined by the flow rule. The shear yield (f^s), tension yield (f^t), and volumetric yield (f^v) functions are given by Equations 3.4 – 3.6. The shear plastic flow

rule is non-associated, whereas tensile and volumetric flow rules are associated as their corresponding potential functions coincide with the yield functions (Equations 3.7 - 3.9).

$$f^s = \sigma_1 - \sigma_3 N_\phi + 2c\sqrt{N_\phi} \tag{3.4}$$

$$f^t = \sigma^t - \sigma_3 \tag{3.5}$$

$$f^v = \frac{1}{3}(\sigma_1 + \sigma_2 + \sigma_3) + p_c \tag{3.6}$$

where $N_\phi = \frac{(1+\sin\phi)}{(1-\sin\phi)}$; ϕ is the friction angle; c is the cohesion; σ^t is the tensile strength; and p_c is the cap pressure.

$$g^s = \sigma_1 - \sigma_3 N_\psi \tag{3.7}$$

$$g^t = -\sigma_3 \tag{3.8}$$

$$g^v = \frac{1}{3}(\sigma_1 + \sigma_2 + \sigma_3) \tag{3.9}$$

Where $N_\phi = \frac{(1+\sin\psi)}{(1-\sin\psi)}$, ψ is the dilation angle.

In the case of yielding, plastic strains are calculated using the flow rules (Equations 3.10 - 3.12) for shear, tensile and volumetric yielding.

$$\Delta e^{ps}{}_i = \lambda^s \frac{\partial g^s}{\partial \sigma_i} \tag{3.10}$$

$$\Delta e^{pt}{}_i = \lambda^t \frac{\partial g^t}{\partial \sigma_i} \tag{3.11}$$

$$\Delta e^{pv}{}_i = \lambda^v \frac{\partial g^v}{\partial \sigma_i} \tag{3.12}$$

where $i = 1,3$ and λ^s, $\lambda^t$and λ^v are constants.

The constitutive models use composite yield functions. For example, in Mohr-Coulomb (MC) model, the composite yield function consists of MC shear yield function and a non-associated shear flow rule along with a tension yield function and an associated tension flow rule (Figure 3.3).

The Mohr-Coulomb strain softening (MCSS) model is used to characterise the post-failure softening behaviour of the rocks. The definition of the MCSS model requires additional parameters in the form of friction, cohesion, dilation, and tension as a function of plastic shear strain. The strength reduction in the rocks after the failure is implemented by reducing the above parameters as a function of evolving plastic strain in the rocks.

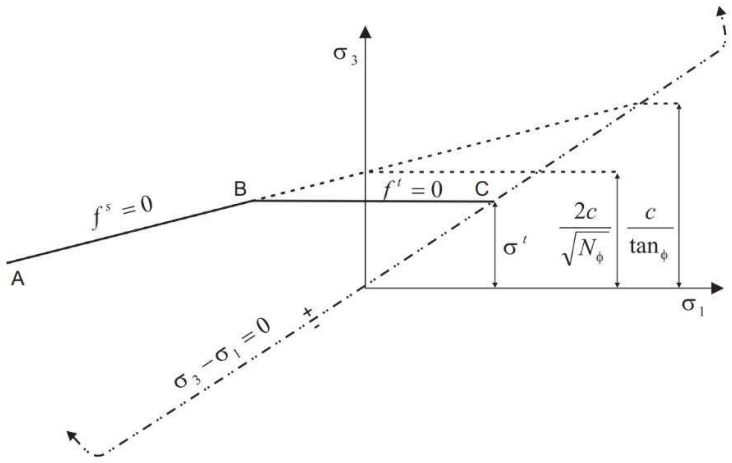

Figure 3.5 Mohr-Coulomb failure criterion with tension cut-off

The Double-yield model was originally developed to model the mechanical constitutive behaviour of the backfill material in the goaf. The model uses composite yield functions, where volumetric yielding is also taken into account by volumetric yield function with associated volumetric flow rule apart from the shear and tensile yield with non-associated shear flow rule and associated tension flow rule, respectively. The cap pressure vs plastic volumetric strain table defines the irreversible volumetric compaction due to isotropic stresses.

In the Ubiquitous joint model, the presence of weak planes is accounted for in the MC material model. The failure along the weakness planes is characterised using the MC yield function with non-associated flow rule and tension yield function with associated flow rules for the joints.

Further, the Ubiquitous joint model requires strength parameters of the joints along with the parameters of the MC model.

3.5.1 Selection of Material Model for Rock Mass

Proper material model selection is essential for modelling the deformation of strata, failure above the excavated area and correct estimation of loads on the surrounding structures. The rock strata exhibit anisotropic elastic deformation before any failure. This behaviour can be captured in FLAC^{3D} using the transversely isotropic constitutive model, which considers independent deformation modulus along and normal to the bedding plane.

The caved, fractured, and Continuous Deformation zones in the damaged overlying strata can be identified based on characteristically different behaviour due to varying intensity of cracks and fractures. The failure of the damaged strata may occur either by joints, stratification, or rock mass. Hence, the anisotropic yield surface better characterises the failure behaviour of these strata. The Ubiquitous-joint model can be used to model this phenomenon.

Since the transversely isotropic model cannot be run together with an anisotropic yield surface in FLAC^{3D} v 5.01, a few assumptions have been made in this study to run the model without compromising the accuracy of the final results. In the Fractured zone, it is assumed that strength features dominate the mechanical behaviour of the strata due to their highly fractured nature. Hence, the anisotropic yield surface presented by the Ubiquitous-joint model was assigned together with the isotropic Elastic model for modelling the deformation of rock mass within this zone. Further, it was also assumed that the deformational aspects of the Continuous Deformation zone are primarily represented by the mechanical behaviour of the rock mass within this zone. Hence, the Transversely Isotropic model was assigned to model the behaviour of strata in the Continuous Deformation zone.

The fragmented rocks in the Caved zone show strain-hardening characteristics when subjected to compressive loading due to the sagging of overlying fractured strata and heaving of the floor strata. The volume of the caved goaf material decreases due to a reduction in the void ratio under the compressive loading. Consequently, the stress and deformation modulus of the goaf material increases progressively. This constitutive behaviour of the goaf material was modelled using the Double-yield model.

When the stress in the rocks exceeds the strength of rock structures, permanent deformation characterised by plastic deformation in continuum mechanics takes place. Accurate modelling of the post-peak strength and deformational behaviour of the rocks is crucial while studying the structural and functional stability of a mining structure. Hence, the MCSS model was used to capture the behaviour of failed and stable coal pillars. The deformational and yield behaviours in this model is defined by the Isotropic Elastic model and the Mohr-Coulomb failure criterion, respectively. The post-failure degradation of the strength is accounted for in the model by shrinkage of the failure envelope, as governed by reduction of friction angle and cohesion of the rocks with the evolving plastic shear strain.

3.5.2 Post-Failure Degradation of Strength Parameters

The post-failure parameters in the MCSS model were determined using the iterative technique to model the stress-strain characteristics of six Indian coal seams. The details of the modelling procedure have been presented in Chapter 4. Based on the modelling results and regression analysis, Equations 4.1 - 4.4 were developed to estimate the post-peak softening parameters.

Walton and Diederichs (2015) dilation angle model (W-D model) was employed to model the post-failure mobilisation of the dilation angle. The model considers the dilation angle as the function of confining stress and plastic shear strain. The peak dilation angle for sedimentary

rocks and their post-mobilisation decay is given by Equations 3.13 and 3.14, respectively. Table 3.2 defines the associated variables.

$$\psi_{Peak}(\sigma_3) = \frac{\phi_{Peak}}{1 + \log_{10}(UCS)} \cdot \log_{10}\left(\frac{UCS}{\sigma_3 + 0.1}\right) \tag{3.13}$$

$$\psi(\sigma_3, \gamma^p) = \begin{cases} \dfrac{\alpha \cdot \gamma^p \cdot \psi_{Peak}}{e^{((\alpha-1)/\alpha)} \cdot \gamma_m} & when \;\; \gamma^p < \gamma_m \cdot e^{((\alpha-1)/\alpha)} \\ \psi_{Peak} \cdot \left(\alpha \cdot \ln\left(\dfrac{\gamma^p}{\gamma_m}\right) + 1\right) & when \;\; \gamma_m \cdot e^{((\alpha-1)/\alpha)} \le \gamma^p < \gamma_m \\ \psi_{Peak} \cdot e^{(-(\gamma^p - \gamma_m)/\gamma^*)} & when \;\; \gamma^p \ge \gamma_m \end{cases} \tag{3.14}$$

where,

$$\alpha = \alpha_0 + \alpha' \cdot \sigma_3 \tag{3.15}$$

$$\gamma^* = \begin{cases} \gamma_0 & when\ \sigma_3 = 0 \\ \gamma' & when\ \sigma_3 \neq 0 \end{cases} \tag{3.16}$$

Table 3.2 Parameters of the W-D dilation angle model (Walton and Diederichs, 2015)

Parameter	Definition
α_0	Determines the curvature of the pr-mobilization portion of the curve for $\sigma_3 = 0$
α'	Determines how the pre-mobilisation curvature changes as a function of σ_3
γ_m	Defines the plastic shear strain at which peak dilation is achieved
γ_0	Defines the decay rate of the dilation angle post-mobilisation for zero confinement
γ'	Defines the decay rate of the dilation angle post-mobilisation for non-zero confinement

3.6 Estimation of the Rock Mass Properties

The deformation and strength properties determined from the laboratory testing of intact rock samples were scaled down by considering the scale effect and heterogeneity present at the field scale to estimate the rock mass properties. The prevalent approaches for reducing intact rock parameters into the rock mass parameters include (i) generalised Hoek and Brown (2002) failure criterion, where the presence of discontinuities is characterised using the Geological Strength Index (GSI); (ii) Sheorey (1997) non-linear failure criterion, where the rock mass

rating (Bieniawski, 1976) is used to account for the presence of discontinuities; (iii) Singh and Singh (2009), where discontinuities and heterogeneity are taken into account by Rock Quality Designation (RQD) and scale effect of 50%; (iv) Mohammad et al. (1997) and Cai et al. (2013) based on the correlation between numerical model properties and laboratory measurements.

Any of these methods can be opted to estimate rock mass properties, provided it is verified to produce correct modelling results in given geo-mining conditions. The Singh and Singh (2009) approach has been verified by comparing the numerical modelling results of the caving behaviour with the field observations and measurements at 27 longwall panels under varying geo-mining conditions in India. Further, the Sheorey (1997) failure criterion has been used by several researchers to study the behaviour of coal pillars in Indian geo-mining conditions, and the results are reported to corroborate well with the field observations and instrumentation data (Mohan et al., 2001).

Accordingly, the Sheorey failure criterion was used in this study to estimate the constitutive parameters associated with the study of the failed and stable cases of coal pillars; the Singh and Singh (2009) approach was used to estimate the rock mass parameters for the rest of the models. The advantage of these criteria is that they require only compressive and tensile strength, RQD, and RMR to determine the rock mass parameters. As most of the longwall workings considered in this study are old and their triaxial properties were not available, these aspects of the criteria were very useful in the present study.

In the approach suggested by Singh and Singh (2009), the compressive and tensile strengths of the rock mass are estimated by downgrading respective laboratory strengths by taking into account the scale effect of 50% and the RQD of the rock strata. The elastic modulus of the rock mass is determined by following the approach suggested by Wilson (1980). In the absence of

triaxial test data, the friction angle for coal and rocks was 25° and 40°, respectively. The dilation angle for coal and rocks was 2° and 5°, respectively.

Sheorey (1997) failure criterion considers the Rock Mass Rating (Bieniaski, 1976) to estimate the strength properties of the rock mass from the laboratory test results (Equation 3.17 - 3.20).

$$S_{3c} = \sigma_{cm}\left(1 + \frac{\sigma_3}{\sigma_{tm}}\right)^{b_m} \tag{3.17}$$

$$\sigma_{cm} = \sigma_c e^{\left(\frac{RMR-100}{20}\right)} \tag{3.18}$$

$$\sigma_{tm} = \sigma_t e^{\left(\frac{RMR-100}{27}\right)} \tag{3.19}$$

$$b_m = b_i^{\left(\frac{RMR}{100}\right)} \tag{3.20}$$

where S_{3c} and σ_3 are triaxial strength and confining stress of the rock mass (MPa); σ_{cm} and σ_c denote the compressive strength of the rock mass and the intact rock, respectively; σ_{tm} and σ_t represent their tensile strength, $'b_i'$ represents the exponent of the failure criterion and is equal to 0.51. The shear strength (τ_{sm}), coefficient of the internal friction angle (μ_{0m}), and the internal friction angle (ϕ_{0m}) are given by the following equations:

$$\tau_{sm} = \left(\sigma_{cm}\sigma_{tm}\frac{{b_m}^{b_m}}{(1+b_m)^{1+b_m}}\right)^{1/2} \tag{3.21}$$

$$\mu_{0m} = \left(\frac{{\tau_{sm}}^2(1+b_m)^2 - {\sigma_{tm}}^2}{2\tau_{sm}\sigma_{tm}(1+b_m)}\right)^{1/2} \tag{3.22}$$

$$\phi_{0m} = \tan^{-1}(\mu_{0m}) \tag{3.23}$$

The cohesion and friction angle so estimated were increased by 10% and decreased by 5°, respectively, for its use as the Mohr-Coulomb strength parameters. These adjustments were obtained by fitting the linear failure envelope of the MC criterion to the non-linear failure

envelope of the Sheorey (1997) criterion. The joint strength parameters for the ubiquitous-joint model were determined using the hit-and-trial technique, whereby the model observed subsidence was calibrated with the field observation in Model VI. The details of this work have been presented in Chapter 6. The determined values of the joint cohesion ($\mathbf{c_j}$) and joint friction (ϕ_j) are 125 kPa and 27°, respectively.

The parameters of the transversely isotropic model were estimated by following a similar approach, as described in Chapter 6. It was assumed that the plane of isotropy is along the 1-2 direction. The elastic modulus e1 = e2 was determined using the Geological Strength Index (GSI) for jointed rock mass. The Shear modulus, g13, was estimated as 33 MPa for Indian geo-mining conditions. The representative value of the ratio of e1 and e3 was obtained as 1.72 for these conditions. The value of nu12 = nu13 was assumed as 0.25 in the models.

3.7 In-situ Stress Field

Due to the unavailability of in-situ stress measurement data for the workings, theoretical approaches were adopted for estimating the pre-mining stresses. The average horizontal stress was estimated using the elasto-static thermal stress model (Sheorey, 1994) (Equation 3.24). This model is reported to fit the measured in-situ stress values worldwide (Sheorey et al., 2001; Singh and Singh, 2009). The vertical in-situ stress was estimated considering the gravity loading (Equation 3.25).

$$\sigma_h = \frac{\nu}{1-\nu}\gamma H + \frac{\beta_T E G_T}{1-\nu}(H + 1000) \tag{3.24}$$

$$\sigma_v = \gamma H \tag{3.25}$$

where, σ_v is the vertical stress (MPa), σ_h is the average horizontal stress (MPa), ν is the Poisson's ratio of the rock, γ is the unit weight of the overburden (MPa/m), H is the cover depth (m), β_T is the coefficient of thermal expansion of the rock ($8\times10^{-6}/^0$C for sandstone and $30\times10^{-5}/^0$C for coal), G_T is the average value of geothermal gradient (0.03^0C/m), and E is Young's modulus of the rock (MPa).

3.8 Two-dimensional Model for Chain Pillar Stability (Model I)

A two-dimensional plane strain model of the vertical section along the face length was created to assess the loading and stability of the chain pillar between two mined-out panels. The mining zone (denoted as 'a') included two longwall faces, the intervening chain pillar, chain pillars on the other side of the longwall faces, and the tailgate and headgate entries (Figure 3.4). The height of the Caved zone (h_c) and Fractured zone (h_f) were considered to be 15 times and 28 times the extraction height (h_e) based on the field measurements in Indian conditions and the works of previous researchers (Section 6.2, Chapter 6). The rock strata in the Fractured zone were assigned the Ubiquitous-joint model, whereas those in the Continuous Deformation zone were assigned the Transversely Isotropic model. The gob material in the Caved zone was modelled using the Double-yield material model. The details of the strength and deformability parameters of these constitutive models are given in Chapter 6.

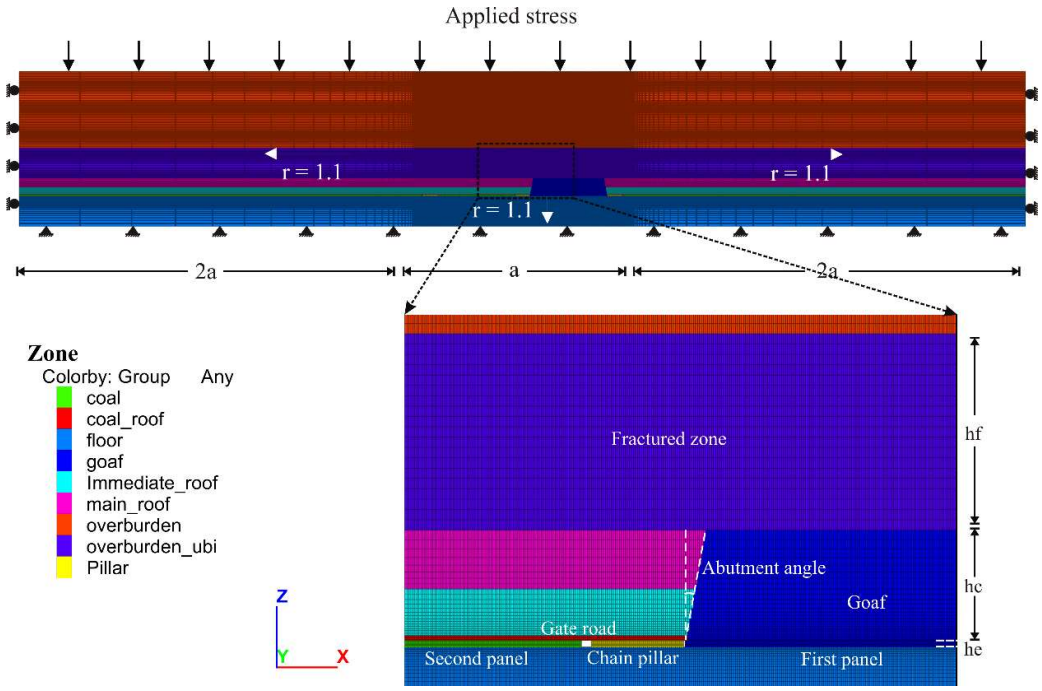

Figure 3.6 The geometry and boundary conditions of the plain-strain model

The element size within the mining zone was kept 1 m × 1 m× 1 m, and increased gradually in the floor by maintaining a Geometrical Progression series ratio of 1.1. A similar ratio was also applied in the x-direction beyond the mining zone. The element size in the roof above the extraction height was kept uniform to simulate mining-induced subsidence in the model. The side boundaries were fixed at a distance of two times the mining zone from the edge of the mining zone to satisfy the condition of the infinite elastic boundary. An overburden thickness of 250 m above the Fractured zone was considered for the models of deep longwall workings. The floor of 200 m thickness was modelled in all such cases. The vertical stress equivalent to the remaining overburden load was applied at the top of the model.

The side boundaries of the model were constrained horizontally by prescribing a roller boundary, while the bottom of the model was specified with a rigid boundary. The contact surfaces between the coal seam-roof strata and the coal seam–floor strata were modelled using

interface elements. The interface stiffness was estimated using the approach discussed in Section 3.3 for Interface type – II. The coal seam was assigned the Elastic constitutive model to evaluate the factor of safety of the pillar. The failure and stress transfer mechanics of the chain pillars were also studied using the strain-softening model for the coal seam in various case studies reported in Chapter 9.

The modelling study was done in three stages to replicate the actual mining process. In the first stage, the virgin elastic model was run to achieve mechanical equilibrium, following which the elastoplastic material models as discussed above were assigned, and the model was further run to the state of equilibrium. All velocities and displacements were initialised to zero before saving the virgin state of the model to represent pre-mining conditions. The gate road entries were developed in the second stage, and the model was solved until it attained mechanical equilibrium. In the third stage, the coal and the rock within the pre-defined Caved zone were instantaneously replaced by the Double-yield material. The models were solved until the model achieved the equilibrium condition.

3.9 Estimation of Rock Mass Parameters for Fractured and Continuous Deformation zones (Model VI)

This model was prepared for a single longwall panel to derive the joint strength parameters of the Ubiquitous-joint model for the Fractured zone and deformability parameters of the Transversely Isotropic model for the Continuous Deformation zone using the bench-marking procedure. This procedure involved calibrating the model to match the subsidence results with the field observed or empirically estimated subsidence using the hit-and-trial technique. Taking advantage of the symmetry condition in the panel, the mining zone (denoted as ‘a/2’) of the model considered only half of the panel width, a chain pillar, and the gate road, thus reducing

the model size for faster convergence of the solution (Fig. 3.5). The models were constructed with the overburden thickness up to the surface.

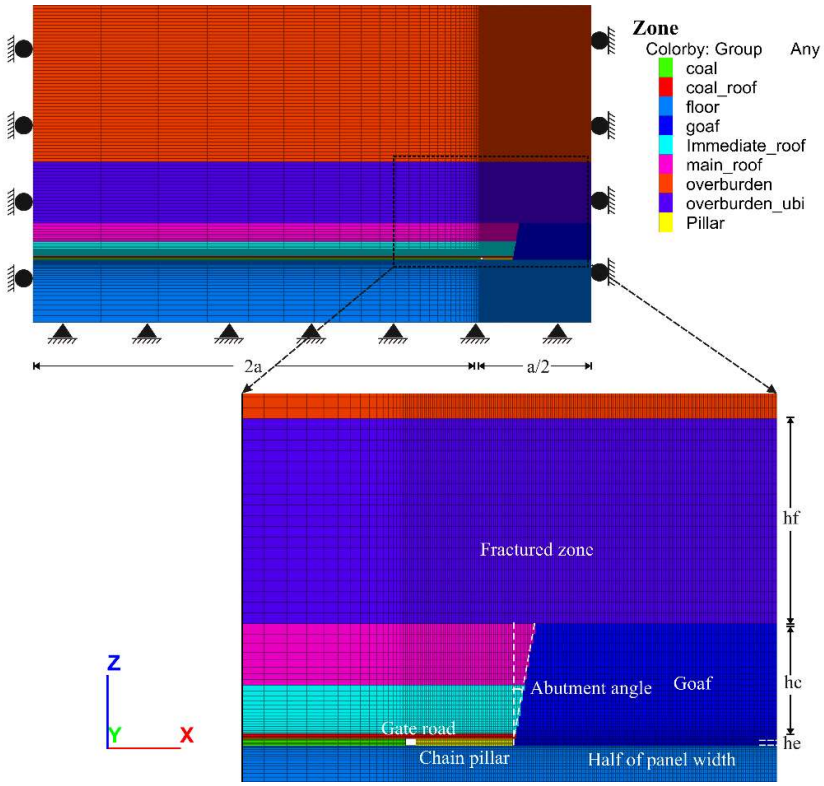

Figure 3.7 The geometry and boundary conditions of the plain-strain model employed to determine the rock mass parameters

3.10 Derivation of the Strain Softening Parameters (Model III)

The post-peak strength parameters of coal were estimated through an attempt to simulate the laboratory observed post-failure behaviour during servo-controlled uniaxial compression tests of coal samples having different width-to-height ratios for six Indian coal seams. A statistical model was proposed to estimate the post-failure strength parameters using the best-fit outcomes of the numerical modelling results.

The numerical model formulation of the coal sample models considered uniform zone size across the volume of the sample and the interface effect. The model geometry considered cylindrical-shaped coal specimen of NX size (diameter of the core, D = 54 mm) and different lengths along with discs-shaped steel platens at the specimen ends. The diameter and thickness of platens were considered to be 55 mm (D+1) and 18mm (D/3), respectively (Bieniawski and Bernede, 1979). The contact surfaces between the specimen and platens were modelled using Coulomb sliding interface elements available in FLAC^{3D}. The FLAC^{3D} grids of the specimens and platens were generated using the meshing plug-in Griddle 2.0 and Rhinoceros 5.0 CAD system (Itasca, 2020), as the basic shape such as radial cylinder available in the FLAC^{3D} was not suitable for discretizing the model of the cylindrical shaped specimen using a uniform grid of almost equal size. The Griddle 2.0 developed by Itasca Consulting Group is used for a wide range of surface meshing and volumetric grid generation in automatic and interactive modes. Rhinoceros 5.0 is a NURBS (Non-Uniform rational basis spline) based 3-D modelling software used to design complex geometries.

The dimensions of the samples and platens were designed using Rhinoceros, and their surfaces were meshed using the unstructured surface mesher tool of Griddle in 'AllQuad mode' to generate pure quadrilateral meshes. The maximum and minimum edge length was set to the desired zone size. Using these quadrilateral surfaces as the boundaries, the unstructured volume mesher function was used to generate conformal hexagonal elements in the model with the desired element size. The output meshes were imported in FLAC^{3D} for further numerical analysis. Figure 3.6 illustrates the geometry of the discretised models of different w/h ratios.

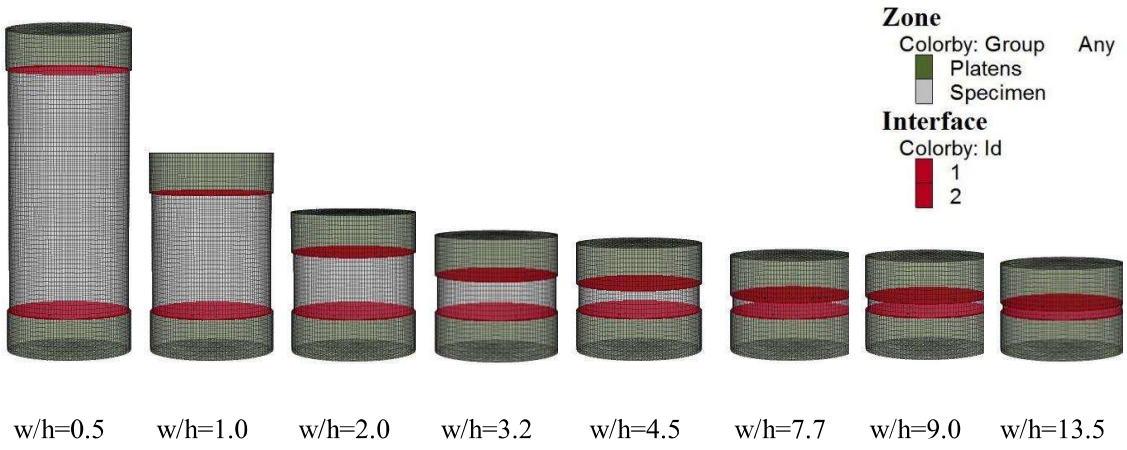

Figure 3.8 Geometry of coal sample models of different diameter to height ratio

Three sets of models with zone sizes of 0.5, 1, and 2 mm were run to evaluate the effect of zone size on the strain-softening behaviour of the model. The horizontal and vertical displacements at the top and bottom of the model were restricted by applying fixed boundary conditions. A constant z-velocity parallel to the specimen axis was applied. The displacement-controlled loading results in compressive stresses throughout the specimen. The confining stresses in the specimen developed due to the shear resistance offered by contact surfaces at the specimen ends. The stiffness of the interface used in this model was estimated using the approach discussed in Section 3.3 for Interface type – II.

FLAC^{3D} solution scheme works on the concept of 'frozen velocity' wherein the neighbouring zones are unaffected when the calculation cycle is performed for the zone under consideration. Hence, the solution scheme requires that a lower velocity is applied at the specimen ends to model the static uniaxial loading process correctly. Contrary to this, the limitation on computational time necessitates the applied velocity to be higher. After several trials, the applied velocity was fixed at $\mathbf{10^{-5}}$mm/timestep as a trade-off between the two conditions. The

details of the iterative modelling scheme to calibrate the model stress-strain curve against the laboratory-obtained curve have been detailed in Chapter 4.

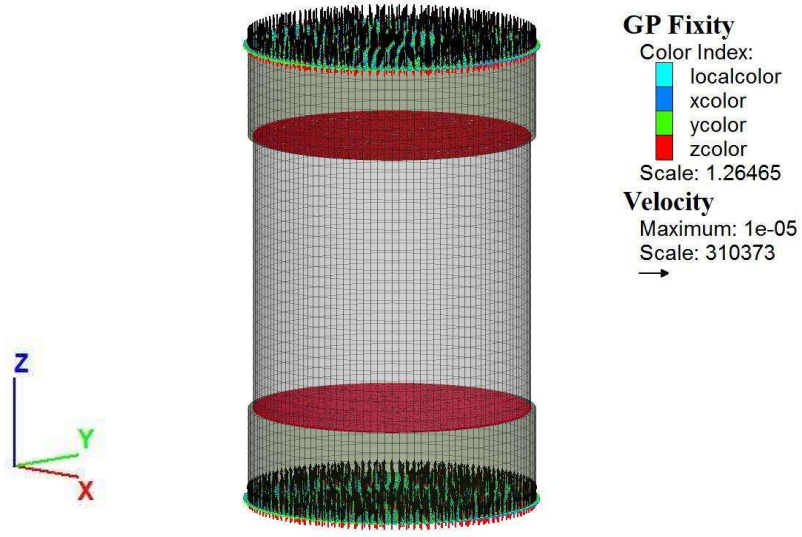

Figure 3.9 Boundary condition for coal sample of w/h=1.0

3.11 Study of Failed and Stable Pillars (Model IV)

In this study, the failed, and the stable cases of pillars from Indian geo-mining conditions were modelled to determine the average factor of safety of the failed pillar cases. The formulation of the pillar model considered the interface effect, post-peak degradation of strength parameters, and mobilisation of the dilation angle. Only a quarter geometry of the pillar was modelled utilising the symmetry condition of the pillar (Figure 3.10). The model considered a 30 m thick floor and the same thickness of the roof in all cases where the cover depth was more than 30 m. The coal pillar was discretised using a uniform zone size of 0.5 m × 0.5 m× 0.5 m. The thickness of the regular-sized brick-shaped elements in the pillar was increased gradually while moving away in the roof and the floor to optimise the computational time and the

modelling accuracy. While roller boundary was prescribed to the side boundaries, fixed boundary condition was assigned at the bottom boundary of the model. During numerical iterations, a constant velocity of $\mathbf{1 \times 10^{-5}}$ m/timestep was applied at the model top. The interface elements were used to simulate the shear resistance due to contact surfaces between the roof and the pillar, and the floor and the pillar.

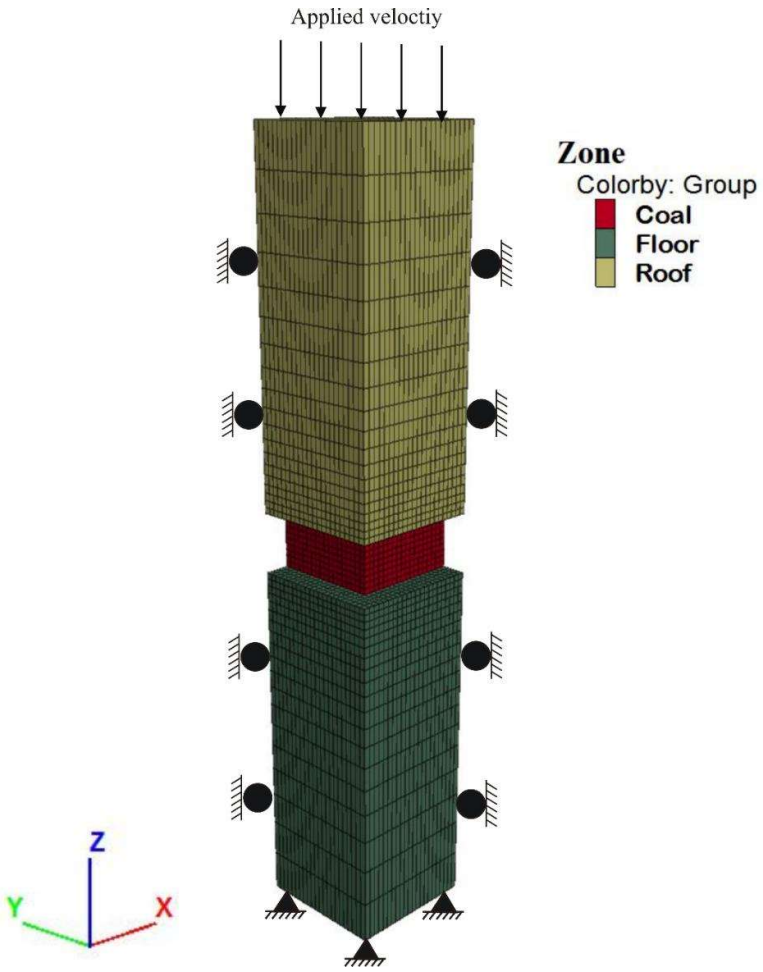

Figure 3.10 Geometry of the pillar model along with its boundary conditions

The roof and floor rock mass were modelled as Elastic materials as the failure was observed to occur only in the pillar. The density of the rock mass was 2500 kg/m^{3,} and the Poisson's ratio

was 0.2. The modulus of rock mass was considered as 7 GPa. The roof-coal and floor-coal contact surfaces were modelled using the interface elements. The stiffness of the interface elements was estimated using the approach discussed in Section 3.3 for Interface type – II, whereas the shear strength properties were estimated based on laboratory tests of Indian rocks (Das et al., 2019).

3.12 Study of Goaf Behaviour Control Parameters (Model II)

A numerical model was prepared to simulate uniaxial compression of goaf material, replicating the laboratory study conducted by Pappas and Mark (1994) (Figures 3.11(a)-(b)). In commensuration with the dimension of the loading chamber used in that study, the numerical model considered a cylindrical sample of 336.5mm in diameter and 304.8mm in height (Figure 3.9c). The roller boundary was prescribed along the periphery, while the rigid boundary was applied at the bottom surface to simulate the restrictions offered by the wall and the fixed base of the test chamber. During numerical iterations, a constant velocity of $\mathbf{1 \times 10^{-6}}$ mm/timestep was applied at the top of the model to simulate the loading of the goaf material in the test chamber by the upper platen of the loading machine. The mechanical response of the model was monitored continuously at every 100 timesteps by recording the history of average vertical stress (σ_v), volumetric strain (e) and accumulated plastic strains (e^{pv} and e^{ps}). This model was employed to determine the cap-pressure table by calibrating the model observed stress-strain characteristic with Salamon's (1990) model. This model is reported to correctly represent the constitutive behaviour of goaf material for different rock types (Pappas and Mark, 1994).

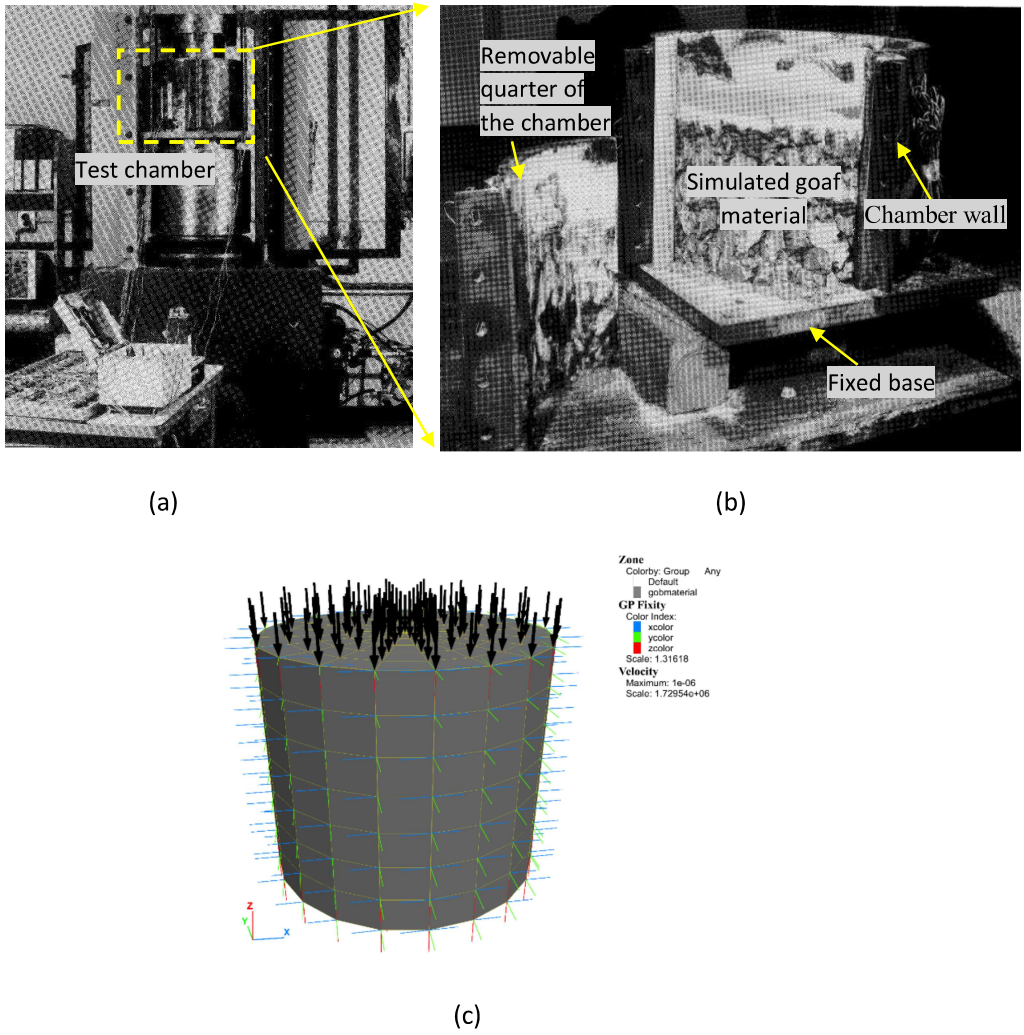

Figure 3.11 Load deformation set up for confined uniaxial testing of graded down goaf material (a); simulated goaf material after completion of the test (b) (after Pappas and Mark 1994); and numerical model for replicating the laboratory tests (c)

3.13 Assessment of Abutment Angle in Longwall Workings (Model V)

Most of the previous works (Mark, 1992; Colwell et al., 1998) considered a constant abutment angle while studying the stability of chain pillars under varying geo-mining conditions. However, several field observations and measurements have suggested that the abutment angle varies with the depth of the seam and the strength and massiveness of the overlying strata (Das, 2000; Lawson et al., 2017). To this end, an independent parametric study using the three-

dimensional modelling environment of FLAC3D was conducted to study the effect of various geo-mining parameters on the abutment angle in the longwall working. The formulation and modelling scheme of the three-dimensional model are the same as reported in Behera et al. (2020a, 2022).

The mining zone in the model considered only half of the face length, a row of chain pillars, and gate entries because of the symmetry conditions. The thickness of the floor considered in the model was 50 m. The model was prepared up to the height of 150 m above the coal seam. The vertical stress equivalent to the weight of the remaining overburden was applied at the top boundary of the model. The uniform zone size of 1 m × 0.75 m× 0.43 m was kept in the mining zone and was increased gradually beyond this zone with a GP ratio of 1.15 along the x and the y- axes and 1.1 along the z-axis. The lateral boundaries of the model were fixed at a distance of two times the panel dimensions from its edge using the roller boundary conditions, whereas the fixed boundary condition was applied at the model bottom. Figure 3.10 illustrates the virgin model.

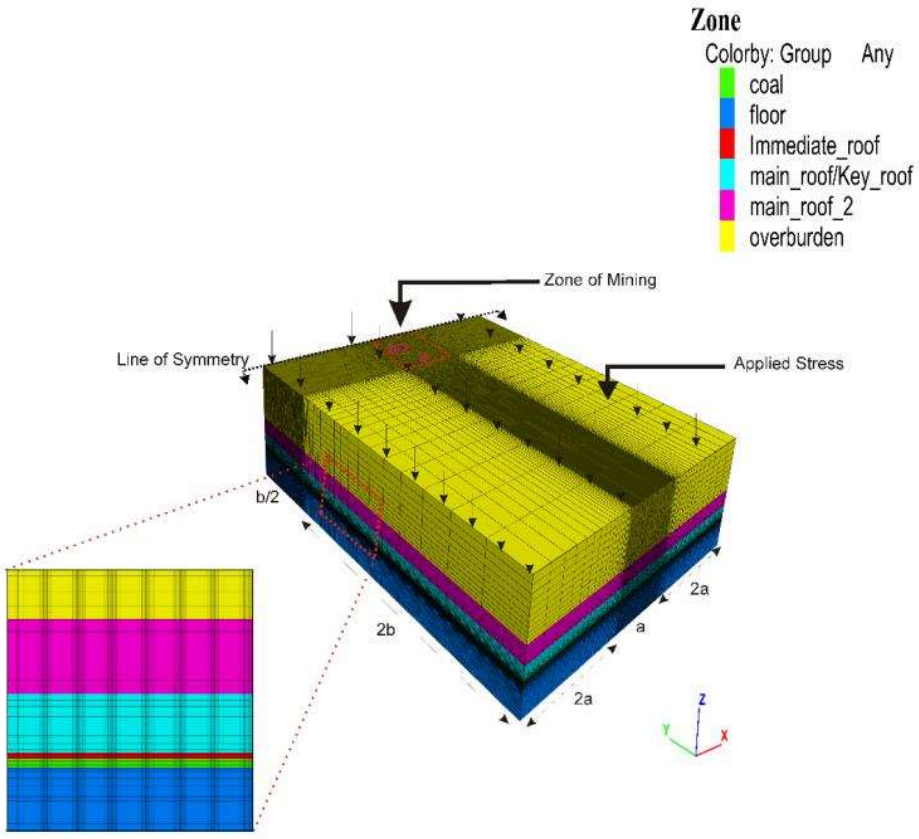

Figure 3.12 Geometric view of the three-dimensional model (Behera, 2022)

The modelling scheme considered field representative progressive advance of the face and caving of the overlying strata. Hence, the interface elements were considered for the simulation of slip and separation along the bedding planes. The interface stiffness was determined using the approach explained in Section 3.3 (Interface type – II). The progressive face advance was simulated in the model in the stages of 1m. The cyclic installation and withdrawal of shield supports were modelled using the concept of the Ground Response Curve (GRC). The canopy and base of the supports were modelled by assigning Elastic constitutive models. The nodal forces were applied at 1 and 3 m behind the face to represent the support reaction. These forces were updated at a fixed interval of time steps based on the displacement at these nodes and the

stiffness of the support. The material properties of the rock strata were determined following the approach suggested by Singh and Singh (2009). The post-failure softening of rock strata in the caving zone during progressive mining was modelled by degrading the cohesion to 20% of its peak value and tensile strength to zero. The caving of the failed zones was ensured based on plastic shear strain and vertical displacement criteria.

3.14 Model for Estimating the Design Criterion for Chain Pillars

A FISH routine was developed to monitor the major and minor principal stresses in every zone of the chain pillar in the elastic plain-strain model I. The stresses were used to evaluate the safety factor of the zones forming the chain pillar, and their average was computed for the given pillar geometry. The factor of safety of a zone was calculated using Equation 3.26 for tensile failure and Equation 3.27 for shear failure.

$$\text{FoS} = \frac{\sigma_t}{\sigma_3} \tag{3.26}$$

$$\text{FoS} = \frac{S_{3c} - \sigma_3}{\sigma_1 - \sigma_3} \tag{3.27}$$

$$S_{3c} = \sigma_3 \cdot \left(\frac{1 + \sin\phi}{1 - \sin\phi}\right) + \frac{2c\cos\phi}{1 - \sin\phi} \tag{3.28}$$

where $\boldsymbol{\sigma_1}$ and $\boldsymbol{\sigma_3}$ are major and minor principal stresses. $\boldsymbol{S_{3c}}$, $\mathbf{c}$, and $\boldsymbol{\phi}$ are triaxial strength, cohesion, and friction angle of the material.

The critical value of the safety factor for the optimum pillar design was estimated based on the back-analysis of failed and stable pillar cases in Indian geo-mining conditions (Chapter 5).

3.15 Summary

A systematic numerical modelling approach was developed in this chapter for a field representative estimation of the load and strength and developing a suitable criterion for the design of chain pillars. A series of numerical modelling studies were carried out to develop essential frameworks for the optimum design of chain pillars, as presented below:

- Modelling of laboratory-scale compression test on graded down caved goaf material to replicate its constitutive behaviour.
- Plain-strain modelling of the single panel for accurate estimation of the extent of Fractured and Continuous Deformation zones above the extracted longwall faces and their constitutive material properties based on the back-analysis of the surface subsidence using the hit-and-trial technique.
- Three-dimensional modelling of caving behaviour of the strata with progressive face advance for estimation of the abutment angle in different geo-mining conditions to accurately estimate the loading of the chain pillars
- Modelling of servo-controlled uniaxial compression tests of coal specimens for various w/h ratios to replicate their post-peak behaviour and obtain their governing rule
- Simulation of the failed and stable pillars in Indian geo-mining conditions to develop a criterion to design optimum size chain pillars. The governing rules developed from these studies were utilised for modelling the softening behaviour.

The formulation of field scale two and three-dimensional models consisted of defining the model geometry, parting planes and boundary conditions, initialising the in-situ stress field, and assigning appropriate constitutive models and their properties for field representative model behaviour. The borehole and laboratory test data were utilised to identify rock beds, different strata in the Caved zone, and rock mass properties.

In the laboratory-scale models, the formulation comprised the model geometry, boundary and loading conditions and assigning proper constitutive model and properties. The simulation schemes involved the replication of the original mining and testing procedures.

The factor of safety of the chain pillar was evaluated using a FISH routine. The routine involved monitoring the major and minor principal stresses to calculate the factor of safety for each zone of the pillar using Equations 3.26 – 3.28. The factor of safety of the pillar was calculated as the average of the factor of safety of all the zones in the pillar.